UNIVERSIDAD DE CONCEPCIÓN

Centro de Investigación en Ingeniería Matemática (CI^{2}MA)

Linearly implicit IMEX schemes for the equilibrium dispersive model of chromatography

Raimund Bürger, Pep Mulet,
Lihki Rubio, Mauricio Sepúlveda

PREPRINT 2017-11

SERIE DE PRE-PUBLICACIONES

Linearly implicit IMEX schemes for the equilibrium dispersive model of chromatography

Raimund Bürger[*,a], Pep Mulet[b], Lihki Rubio[a], Mauricio Sepúlveda[a]

[a] *CI²MA & Departamento de Ingeniería Matemática, Universidad de Concepción, Casilla 160-C, Concepción, Chile*
[b] *Departament de Matemàtiques, Universitat de València, Av. Dr. Moliner 50, E-46100 Burjassot, Spain*

Abstract

Numerical schemes for the nonlinear equilibrium dispersive (ED) model for chromatographic processes with adsorption isotherms of Langmuir type are proposed. This model consists of a system of nonlinear, convection-dominated partial differential equations. The nonlinear convection gives rise to sharp moving transitions between concentrations of different solute components. This property calls for numerical methods with shock capturing capabilities. Based on results by [R. Donat, F. Guerrero and P. Mulet (2017); submitted], conservative, shock capturing, numerical schemes can be designed for this chromatography model. Since explicit schemes for diffusion problems can pose severe stability restrictions on the time step, the novel schemes treat diffusion implicitly and convection explicitly. To avoid the need to solve the nonlinear systems appearing in the implicit treatment of the nonlinear diffusion, second-order linearly implicit implicit-explicit (IMEX) Runge-Kutta schemes are employed. Numerical experiments demonstrate that the schemes give accurate numerical solutions with the same stability restrictions as in the purely hyperbolic case.

Key words: Chromatography, Equilibrium Dispersive model, Convection-diffusion equation, Implicit-explicit methods

[*]Corresponding author.
Email addresses: rburger@ing-mat.udec.cl (Raimund Bürger), mulet@uv.es (Pep Mulet), lrubio@ing-mat.udec.cl (Lihki Rubio), mauricio@ing-mat.udec.cl (Mauricio Sepúlveda)

April 30, 2017

1. Introduction

1.1. Scope

Chromatography is used to separate complex fluid mixtures, when a high purity of the product is demanded. In liquid batch chromatography, a pulse of fluid mixture, the solute, is injected at one end of a long cylindrical column filled with a porous medium (the stationary phase), followed by a continuous flow of liquid, the mobile phase, along the column. The solute interacts with the porous medium and its components begin to separate according to the strength of their affinity with the stationary phase. If the column is long enough, band profiles of single components move through it, so making it possible to collect pure fractions of components at its end.

The Equilibrium Dispersive (ED) model [12, 17, 23] is applicable when the mass transfer kinetics between the mobile phase and the stationary phase is fast, and when all band-broadening effects can be lumped into an apparent dispersion coefficient D_{a}. Within the ED model, chromatographic processes can be modeled by first-order non-linear convection-dominated conservation laws [12, 20, 21], coupled with some algebraic relations between the concentrations of the components of the mixture in the mobile and solid phases. Since analytical solutions can seldom be obtained, it is crucial to design numerical schemes for performing simulations with these models, and thereby to help practitioners to reduce the need for costly empirical experimentation.

There are other approaches that take into account the kinetics between the mobile phase and the stationary phase assuming that the equilibrium is not instantaneous, obtaining systems of equations with relaxation terms [13, 14] (see also [12] for a more physical description). Both models (ED and relaxation) are similar when this relaxation parameter tends to zero.

Nonlinear convection terms cause sharp moving transitions between concentrations of different solute components and numerical methods should be able to cope with this situation, i.e., be conservative. Several works of simulation in chromatography propose conservative numerical schemes in which if D_α is null, then the roles of time t and of position z can be interchanged, being then the amounts conserved given by concentration in the mobile phase, and the flux given by the total solute concentrations (see [12, 22]). These schemes are efficient and even used to solve certain problems of identification of parameters in chromatography [16] since they do not require the inversion of the non-linear function that algebraically connects these two concentration vectors (total concentration and mobile phase concentration). The problem

with these schemes is that, on the one hand, they do not conserve the original quantities, i.e., the total concentrations, and on the other hand, they can not apply if $D_\alpha > 0$. In this sense it is proposed in [17] to suitably rewrite the model including the diffusion term and to solve it numerically by a non-conservative, linearized scheme in order to obtain an efficient method. However, Donat et al. [7] show that the non-conservative scheme proposed by Javeed et al. [17] for the simulation of the ED model can yield simulations for which the chromatographic fronts, that correspond to shocks when diffusion is neglected, move at a wrong speed and individual solute concentrations are not conserved when they should.

The main difficulty in the design of conservative numerical schemes in this formulation is that the conversion from conserved variables to primitive variables (concentration of solute and mobile phase) can only be achieved through an implicit function whose properties can be deduced from the mathematical structure of the adsorption isotherm. Nevertheless this implicit function can be approximated numerically by efficient root finders.

The particular structure of the ED model [7], summarized in the next section, provides the theoretical background to implement conservative spatial semi-discretizations of the ED model (1.2), in a method of lines strategy. It is the purpose of this paper to advance fully discrete conservative numerical schemes that are obtained by applying suitable time integrators to the spatial semi-discretization. Explicit schemes applied to diffusion problems can strongly restrict the time step due to stability constraints. Therefore we aim to treat diffusion implicitly and convection explicitly. To avoid the necessity to solve nonlinear systems appearing in the implicit treatment of the nonlinear diffusion [4], we propose second-order linearly implicit IMEX Runge-Kutta schemes recently introduced in [1].

1.2. The Equilibrium Dispersive (ED) model of chromatography

We denote time by t and let z be the axial coordinate along the column that is normalized to have unit height, so that the top is at $z = 0$ and the bottom at $z = 1$. We assume that ε is the constant total porosity of the solid phase, i.e., the proportion of void space that can be occupied by fluid and u is the (constant) velocity of the mobile phase.

We denote by c_i the concentrations of the i-th liquid phase and by q_i the concentration of solid phase adsorbent permeated by the i-th phase. Thus, the total amount of liquid/solid material occupied by the i-th phase is $\varepsilon c_i + (1-\varepsilon) q_i$. The flux for the i-th phase is postulated as $\varepsilon(uc_i - D_\mathrm{a}\partial c_i/\partial z)$,

so that the continuity equations of the ED model can be written as

$$\frac{\partial}{\partial t}\big(\varepsilon c_i + (1-\varepsilon)q_i\big) + \frac{\partial}{\partial z}\left(\varepsilon\left(uc_i - D_{\mathrm{a}}\frac{\partial c_i}{\partial z}\right)\right) = 0, \quad i = 1, \ldots, N. \tag{1.1}$$

We assume that the mobile phase corresponds to the last index N. With the notation $\boldsymbol{c} := (c_1, \ldots, c_N)^{\mathrm{T}}$ and $\boldsymbol{q} := (q_1, \ldots, q_N)^{\mathrm{T}}$ and dividing (1.1) by ε, we obtain the system of continuity equations in the form

$$\frac{\partial}{\partial t}\left(\boldsymbol{c} + \frac{1-\varepsilon}{\varepsilon}\boldsymbol{q}\right) + u\frac{\partial \boldsymbol{c}}{\partial z} = D_{\mathrm{a}}\frac{\partial^2 \boldsymbol{c}}{\partial z^2}. \tag{1.2}$$

Appropriate boundary conditions for this model are proposed in [12], namely

$$u\boldsymbol{c} - D_{\mathrm{a}}\frac{\partial \boldsymbol{c}}{\partial z}\bigg|_{z=0} = u\boldsymbol{c}_{\mathrm{inj}}(t), \qquad \frac{\partial \boldsymbol{c}}{\partial z}\bigg|_{z=1} = 0, \tag{1.3}$$

for a known function $\boldsymbol{c}_{\mathrm{inj}}(t)$ that models the continuous injection of the liquid phases (components 1 to $N-1$) and the "displacer" (component N) through the top of the column.

Within the ED model, the equilibrium relationship between the solid phase and liquid phase concentrations is given by the adsorption isotherm $\boldsymbol{q} = \boldsymbol{q}(\boldsymbol{c})$, which is usually a non-linear function [12]. In this paper we consider multi-component mixtures for which the adsorption isotherms are of Langmuir type, that is

$$q_i = \frac{\alpha_i c_i}{1 + \boldsymbol{\beta}^{\mathrm{T}}\boldsymbol{c}}, \qquad i = 1, \ldots, N, \tag{1.4}$$

where $\boldsymbol{\alpha} := (\alpha_1, \ldots, \alpha_N)^{\mathrm{T}}$, $\boldsymbol{\beta} := (\beta_1, \ldots, \beta_N)^{\mathrm{T}}$, and the constants $\alpha_i, \beta_i > 0$ quantify the nonlinearity of the isotherm. This Langmuir isotherm [18] has the particularity of being a monotonous and concave function in each component, and is based on thermodynamic statistical models of multicomponent phase equilibrium. If we add terms that consider internal energies by grouping the particles in each phase, the model generalizes to isotherms not necessarily concave [12, 15] and considered in models of chromatography for example in [3].

In [7] the theoretical results about the well-posedness of the ED model (hyperbolicity when $D_{\mathrm{a}} = 0$ and parabolicity when $D_{\mathrm{a}} > 0$) obtained in [20] for $N = 1$ are generalized to $N > 1$, see Section 2.

The ED model (1.2) can be written as the system of conservation laws

$$\frac{\partial \boldsymbol{w}}{\partial t} + \frac{\partial (u\boldsymbol{c})}{\partial z} = D_{\mathrm{a}} \frac{\partial^2 \boldsymbol{c}}{\partial z^2}, \quad \text{where } \boldsymbol{w} := \boldsymbol{W}(\boldsymbol{c}) := \boldsymbol{c} + \frac{1-\varepsilon}{\varepsilon}\boldsymbol{q}(\boldsymbol{c}). \tag{1.5}$$

This system can be written in standard form as long as there is a one-to-one correspondence between the variables $\boldsymbol{w}$ and the concentrations $\boldsymbol{c}$. Then, a conservative discretization of the terms with spatial derivatives guarantees mass conservation for the conserved variables $\boldsymbol{w}$, and, as a consequence, the shock-capturing property, i.e. shocks (for $D_{\mathrm{a}} = 0$) or steep profiles (for $D_{\mathrm{a}} > 0$) in the numerical solution propagate at the correct speed.

In [7] it is shown that there is indeed a globally well-defined, one-to-one correspondence between $\boldsymbol{c}$ and $\boldsymbol{w}$, so that (1.5) can be rewritten as

$$\frac{\partial \boldsymbol{w}}{\partial t} + \frac{\partial \boldsymbol{f}(\boldsymbol{w})}{\partial z} = D_{\mathrm{a}} \frac{\partial^2 \boldsymbol{C}(\boldsymbol{w})}{\partial z^2}, \qquad \boldsymbol{f}(\boldsymbol{w}) = u\boldsymbol{C}(\boldsymbol{w}), \tag{1.6}$$

where $\boldsymbol{C}(\boldsymbol{w})$ is a continuously differentiable function that satisfies $\boldsymbol{C} = \boldsymbol{W}^{-1}$. Furthermore, although there is no explicit expression for the function $\boldsymbol{C}(\boldsymbol{w})$ for $N > 1$, the value of $\boldsymbol{C}(\boldsymbol{w})$ for any $\boldsymbol{w} \neq 0$, $w_i \geq 0$ can be determined by computing the only positive root of a particular rational function [7].

1.3. Outline of the paper

The remainder of the paper is organized as follows. In Section 2 we recall from [7] results related to the analysis of the mathematical structure of the ED model. Section 3 describes second-order linearly implicit IMEX Runge-Kutta schemes and discusses some issues required for their implementation in numerical simulations of chromatographic processes that fit the ED model (1.4), (1.5). In Section 4 we show some numerical experiments to test the performance of these schemes. Some conclusions are collected in Section 5.

2. Mathematical structure of the ED model

In what follows we shall assume that the components of the mixture are ordered so that $0 < \alpha_1 < \alpha_2 < \ldots < \alpha_N$, see (1.4). We quote here the main results from [7, 8] that will be needed in the sequel.

Theorem 2.1. *For any $\boldsymbol{c} \in \mathbb{R}^N_+$, the Jacobian matrix $\boldsymbol{W}'(\boldsymbol{c})$ is diagonalizable, with real, strictly positive, pairwise distinct eigenvalues $\lambda_1, \ldots, \lambda_N$ satisfying*

$$1 < \lambda_1 < d_1 < \lambda_2 < \cdots < d_{N-1} < \lambda_N < d_N, \quad d_i := 1 + \frac{\eta_i}{1 + \boldsymbol{\beta}^{\mathrm{T}} \boldsymbol{c}},$$

where $\eta_i := (1 - \varepsilon)\alpha_i/\varepsilon$ for $i = 1, \ldots, N$.

Lemma 2.1. *For any fixed $\boldsymbol{w} \in \mathbb{R}^N_+$, the rational function*

$$\mathbb{R} \ni y \mapsto R_{\boldsymbol{w}}(y) := 1 - y + \sum_{i=1}^{N} \frac{y}{y + \eta_i} \beta_i w_i \in \mathbb{R}$$

has only one positive root, denoted by $\rho_0(\boldsymbol{w})$. In fact, $1 \le \rho_0(\boldsymbol{w}) \le 1 + \boldsymbol{\beta}^{\mathrm{T}} \boldsymbol{w}$.

Theorem 2.2. *The function $\boldsymbol{W} : \mathbb{R}^N_+ \to \mathbb{R}^N_+$ given in (1.5) is invertible. The inverse function $\boldsymbol{C} := \boldsymbol{W}^{-1} \colon \mathbb{R}^N_+ \to \mathbb{R}^N_+$ is continuously differentiable in $\mathbb{R}^N_+$ and is given by $\boldsymbol{C} = (C_1(\boldsymbol{w}), \ldots, C_N(\boldsymbol{w}))^{\mathrm{T}}$, where*

$$C_i(\boldsymbol{w}) := \frac{w_i}{1 + \eta_i/\rho_0(\boldsymbol{w})}, \quad i = 1, \ldots, N.$$

Corollary 2.1. *The ED model (1.6) is well posed in the following sense. For $D_{\mathrm{a}} = 0$ the system of conservation laws*

$$\frac{\partial \boldsymbol{w}}{\partial t} + \frac{\partial \boldsymbol{f}(\boldsymbol{w})}{\partial z} = \boldsymbol{0}$$

is strictly hyperbolic, and for any $\boldsymbol{w}$ such that $w_i > 0$, all the eigenvalues μ_j of its Jacobian matrix $u\boldsymbol{C}'(\boldsymbol{w})$ are positive, pairwise distinct, and bounded above by u. These eigenvalues $\mu_j = u/\lambda_j$ satisfy

$$u > \mu_1 > u/d_1 > \mu_2 > \cdots > u/d_{N-1} > \mu_N > u/d_N > 0$$

(cf. Theorem 2.1). For $D_{\mathrm{a}} > 0$, the system (1.6) is parabolic in the sense of Petrovskii (cf., e.g., [9]), i.e., the eigenvalues of the matrix $D_{\mathrm{a}}\boldsymbol{C}'(\boldsymbol{w})$ are bounded below by some positive constant for any $\boldsymbol{w} \in \mathbb{R}^N_+$.

3. Linearly implicit IMEX schemes

3.1. Method of lines approach

In order to apply this technique to the ED model, we rewrite (1.6) as

$$\frac{\partial \boldsymbol{w}}{\partial t} + \frac{\partial}{\partial z}\left(\boldsymbol{f}(\boldsymbol{w}) - \boldsymbol{g}\left(\boldsymbol{w}, \frac{\partial \boldsymbol{w}}{\partial z}\right)\right) = 0, \quad \boldsymbol{g}\left(\boldsymbol{w}, \frac{\partial \boldsymbol{w}}{\partial z}\right) := D_{\mathrm{a}}\boldsymbol{C}'(\boldsymbol{w})\frac{\partial \boldsymbol{w}}{\partial z}. \tag{3.1}$$

We consider a uniform mesh with grid points $z_j = (j - 1/2)\Delta z$, $j = 1, \ldots, M$, where $\Delta z = 1/M$, and write the resulting semi-discrete scheme as

$$\boldsymbol{w}'(t) = \boldsymbol{\mathcal{L}}\big(\boldsymbol{w}(t)\big) + \boldsymbol{\mathcal{D}}\big(\boldsymbol{w}(t)\big),$$

where $\boldsymbol{w}(t)$ is an $M \times N$ matrix whose j-th column, $\boldsymbol{w}_j(t)$, is an approximation of $w(z_j, t) \in \mathbb{R}^N$, $j = 1, \ldots, M$, $\boldsymbol{\mathcal{L}}$ represents the spatial discretization of the convective term $-\partial \boldsymbol{f}(\boldsymbol{w})/\partial z$ and $\boldsymbol{\mathcal{D}}$ the spatial discretization of the diffusion term $\partial \boldsymbol{g}(\boldsymbol{w}, \partial \boldsymbol{w}/\partial z)/\partial z$ in (3.1).

The schemes we propose compute numerical approximations to the point-values of the conserved variables, $\boldsymbol{w}_j(t) \approx \boldsymbol{w}(x_j, t)$, and are characterized by a conservative discretization of the convective and diffusive terms of the form

$$\boldsymbol{\mathcal{L}}_j = -\frac{1}{\Delta z}\big(\hat{\boldsymbol{f}}_{j+1/2} - \hat{\boldsymbol{f}}_{j-1/2}\big), \quad \boldsymbol{\mathcal{D}}_j = \frac{1}{\Delta z}\big(\hat{\boldsymbol{g}}_{j+1/2} - \hat{\boldsymbol{g}}_{j-1/2}\big)$$

(dropping the dependencies for simplicity), using convective and diffusive numerical fluxes $\hat{\boldsymbol{f}}_{j+1/2}$ and $\hat{\boldsymbol{g}}_{j+1/2}$, respectively, that approximate the respective exact fluxes at the corresponding cell interface $z_{j+1/2} = z_j + \Delta z/2$.

The convective numerical flux

$$\hat{\boldsymbol{f}}_{j+1/2} = \hat{\boldsymbol{f}}(\boldsymbol{w}_{j-1}, \boldsymbol{w}_j, \boldsymbol{w}_{j+1}) \tag{3.2}$$

is computed by MUSCL reconstructions [24] as follows, where we take into account that all characteristic velocities are positive (see Corollary 2.1):

$$\begin{aligned} \hat{\boldsymbol{f}}_{j+1/2} &= u\boldsymbol{C}(\boldsymbol{w}^{\mathrm{L}}_{j+1/2}), \\ \boldsymbol{w}^{\mathrm{L}}_{i,j+1/2} &:= \boldsymbol{w}_{i,j} + \frac{1}{2}\,\mathrm{minmod}(\boldsymbol{w}_{i,j} - \boldsymbol{w}_{i-1,j}, \boldsymbol{w}_{i+1,j} - \boldsymbol{w}_{i,j}), \end{aligned} \tag{3.3}$$

where we use the standard definition

$$\mathrm{minmod}(a, b) := \begin{cases} \mathrm{sgn}(a)\min\{|a|, |b|\} & \text{if } \mathrm{sgn}(a) = \mathrm{sgn}(b), \\ 0 & \text{otherwise.} \end{cases}$$

The diffusive numerical fluxes are computed by second-order centered finite differences

$$\begin{aligned}\hat{\boldsymbol{g}}_{j+1/2} &= \frac{1}{\Delta z}\boldsymbol{B}_{j+1/2}(\boldsymbol{w})(\boldsymbol{w}_{j+1}-\boldsymbol{w}_j),\\ \boldsymbol{B}_{j+1/2}(\boldsymbol{w}) &:= \boldsymbol{B}(\boldsymbol{w}_j,\boldsymbol{w}_{j+1}) = \frac{D_{\mathrm{a}}}{2}\big(\boldsymbol{C}'(\boldsymbol{w}_{j+1})+\boldsymbol{C}'(\boldsymbol{w}_j)\big).\end{aligned} \tag{3.4}$$

The boundary conditions (1.3) at $z = 0 = z_{1/2}$ are discretized by prescribing the sum of convective and diffusive numerical fluxes as follows:

$$\hat{\boldsymbol{f}}_{1/2} - \hat{\boldsymbol{g}}_{1/2} = u\boldsymbol{c}_{\mathrm{inj}}(t) = \boldsymbol{f}(\boldsymbol{w}) - \boldsymbol{g}\left(\boldsymbol{w}, \frac{\partial \boldsymbol{w}}{\partial z}\right)\Big|_{z=0}.$$

The term $\mathcal{L}_1 + \mathcal{D}_1$ is modified accordingly:

$$\begin{aligned}\boldsymbol{\mathcal{L}}_1 + \boldsymbol{\mathcal{D}}_1 &= \frac{1}{\Delta z}\Big(\big(-\hat{\boldsymbol{f}}_{3/2}+\hat{\boldsymbol{g}}_{3/2}\big) - \big(-\hat{\boldsymbol{f}}_{1/2}+\hat{\boldsymbol{g}}_{1/2}\big)\Big)\\ &= \frac{1}{\Delta z}\big(-\hat{\boldsymbol{f}}_{3/2}+\hat{\boldsymbol{g}}_{3/2}+u\boldsymbol{c}_{\mathrm{inj}}(t)\big).\end{aligned}$$

The boundary conditions (1.3) at $z = 1 = z_{M+1/2}$ are discretized by taking

$$\hat{\boldsymbol{g}}_{M+1/2} = \boldsymbol{0} = \boldsymbol{g}\left(\boldsymbol{w}, \frac{\partial \boldsymbol{w}}{\partial z}\right)\Big|_{z=1},$$

so the term $\mathcal{L}_M + \mathcal{D}_M$ is modified accordingly:

$$\begin{aligned}\boldsymbol{\mathcal{L}}_M + \boldsymbol{\mathcal{D}}_M &= \frac{1}{\Delta z}\Big(\big(-\hat{\boldsymbol{f}}_{M+1/2}+\hat{\boldsymbol{g}}_{M+1/2}\big) - \big(-\hat{\boldsymbol{f}}_{M-1/2}+\hat{\boldsymbol{g}}_{M-1/2}\big)\Big)\\ &= \frac{1}{\Delta z}\big(\hat{\boldsymbol{f}}_{M-1/2}-\hat{\boldsymbol{f}}_{M+1/2}-\hat{\boldsymbol{g}}_{M-1/2}\big).\end{aligned}$$

Furthermore, the computation of the convective fluxes as in (3.2), for $j = 2, M$ requires values at the corresponding ghost cells z_k, whose indices are $k = 0$ for the first case and $k = M + 1$ for the second. We obtain the values at those ghost cells by using extrapolation with a linear polynomial that satisfies the boundary condition and that interpolates the data for the internal point which is symmetric with respect to the boundary. For $z = 0$ and $k = 1 - j$, taking into account (1.3), this extrapolation yields the value

$$\boldsymbol{c}_{1-j}(t) = -\boldsymbol{c}_j(t) + \frac{2(j-1/2)h}{(j-1/2)\,h + D_{\mathrm{a}}/u}\boldsymbol{c}_{\mathrm{inj}}(t).$$

For $z = 1$ and $k = M + 1$, in view of (1.3) we obtain by extrapolation

$$\boldsymbol{c}_{M+1}(t) = \boldsymbol{c}_M(t).$$

With all these comments and the notation in (3.4) we can write the resulting spatial semi-discretization as

$$\frac{\mathrm{d}}{\mathrm{d}t}\boldsymbol{U}(t) = \boldsymbol{\mathcal{L}}(\boldsymbol{U}, t) + \boldsymbol{\mathcal{D}}(\boldsymbol{U}), \tag{3.5}$$

where

$$\boldsymbol{U}(t) = \begin{pmatrix} \boldsymbol{w}_1(t) \\ \boldsymbol{w}_2(t) \\ \vdots \\ \boldsymbol{w}_M(t) \end{pmatrix}, \quad \boldsymbol{\mathcal{L}}(\boldsymbol{U}, t) = \begin{pmatrix} \boldsymbol{\mathcal{L}}_1(\boldsymbol{U}, t) \\ \boldsymbol{\mathcal{L}}_2(\boldsymbol{U}, t) \\ \vdots \\ \boldsymbol{\mathcal{L}}_M(\boldsymbol{U}, t) \end{pmatrix}, \quad \boldsymbol{\mathcal{D}}(\boldsymbol{U}) = \frac{1}{\Delta z^2}\boldsymbol{\mathcal{B}}(\boldsymbol{U})\boldsymbol{U},$$

where the sub-vectors $\boldsymbol{\mathcal{L}}_1, \ldots, \boldsymbol{\mathcal{L}}_M$ are given by

$$\boldsymbol{\mathcal{L}}_j(\boldsymbol{U}, t) = \frac{1}{\Delta z}\begin{cases} -\hat{\boldsymbol{f}}_{j+1/2}(\boldsymbol{U}) + \hat{\boldsymbol{f}}_{j-1/2}(\boldsymbol{U}) & \text{for } 1 < j < M, \\ -\hat{\boldsymbol{f}}_{3/2}(\boldsymbol{U}) + u\boldsymbol{c}_{\mathrm{inj}}(t) & \text{for } j = 1, \\ \hat{\boldsymbol{f}}_{M-1/2}(\boldsymbol{U}) & \text{for } j = M, \end{cases}$$

and $\boldsymbol{\mathcal{B}}$ is an $\mathbb{R}^{(NM)\times(NM)}$ block tridiagonal matrix function formed of blocks $\boldsymbol{B}_{j+1/2} \in \mathbb{R}^{N\times N}$ such that

$$\big(\boldsymbol{\mathcal{B}}(\tilde{\boldsymbol{U}})\boldsymbol{U}\big)_j = \begin{cases} \boldsymbol{B}_{j+1/2}(\tilde{\boldsymbol{U}})(\boldsymbol{w}_{j+1} - \boldsymbol{w}_j) \\ \qquad -\boldsymbol{B}_{j-1/2}(\tilde{\boldsymbol{U}})(\boldsymbol{w}_j - \boldsymbol{w}_{j-1}) & \text{for } 1 < j < M, \\ \boldsymbol{B}_{3/2}(\tilde{\boldsymbol{U}})(\boldsymbol{w}_2 - \boldsymbol{w}_1) & \text{for } j = 1, \\ -\boldsymbol{B}_{M-1/2}(\tilde{\boldsymbol{U}})(\boldsymbol{w}_M - \boldsymbol{w}_{M-1}) & \text{for } j = M. \end{cases}$$

The approximate solution of (3.5) can be obtained by the application of Runge-Kutta ODE solvers. Strong Stability Preserving (SSP) explicit Runge-Kutta methods are a popular class of time integrators whose use leads to the following stability constraint (see [6] for details):

$$\Delta t\left(\frac{u}{\Delta z} + \frac{2D_{\mathrm{a}}}{\Delta z^2}\right)\max_{\boldsymbol{U}} \varrho\big(\boldsymbol{C}'(\boldsymbol{U})\big) \le C_0 \le 1 \quad \text{for some constant } C_0 > 0,$$

where $\varrho(\boldsymbol{C}'(\boldsymbol{U}))$ is the spectral radius of $\boldsymbol{C}'(\boldsymbol{U})$. Since $\max_{\boldsymbol{U}} \varrho(\boldsymbol{C}'(\boldsymbol{U})) < 1$, a practical bound would be

$$\Delta t \left(\frac{u}{\Delta z} + \frac{2D_{\mathrm{a}}}{\Delta z^2} \right) \leq C_0 \tag{3.6}$$

This restriction on Δt can be very stringent if D_{a} is not very small or Δz is very small. This restriction originates from the explicit treatment of the diffusion term.

An alternative to explicit Runge-Kutta methods are implicit-explicit Runge-Kutta (IMEX-RK) methods (see [1] and references therein), for which only the diffusion term is treated implicitly. It is hoped (and can be proven in some cases) that the stability restrictions on Δt are of the form

$$\Delta t \frac{u}{\Delta z} \max_{w} \varrho(\boldsymbol{C}'(\boldsymbol{w})) \leq C_1 \leq 1,$$

or, from a practical point of view,

$$\Delta t \frac{u}{\Delta z} \leq C_1. \tag{3.7}$$

An IMEX-RK method is specified by the pair of Butcher arrays

$$\begin{array}{c|c} \tilde{\boldsymbol{c}} & \tilde{\boldsymbol{A}} \\ \hline & \tilde{\boldsymbol{b}}^{\mathrm{T}} \end{array} \qquad \begin{array}{c|c} \boldsymbol{c} & \boldsymbol{A} \\ \hline & \boldsymbol{b}^{\mathrm{T}} \end{array},$$

where the $s \times s$ lower triangular matrices $\tilde{\boldsymbol{A}} = (\tilde{a}_{ij})$ (with $\tilde{a}_{ij} = 0$ for all $j \geq i$) and $\boldsymbol{A} = (a_{ij})$ are the matrices of the explicit and implicit parts of the method, respectively, while $\tilde{\boldsymbol{b}} = (\tilde{b}_1, \ldots, \tilde{b}_s)^{\mathrm{T}}$, $\tilde{\boldsymbol{c}} = (\tilde{c}_1, \ldots, \tilde{c}_s)^{\mathrm{T}}$, $\boldsymbol{b} = (b_1, \ldots, b_s)^{\mathrm{T}}$ and $\boldsymbol{c} = (c_1, \ldots, c_s)^{\mathrm{T}}$ are s-dimensional vectors of real coefficients, and $\tilde{\boldsymbol{c}}$ and $\boldsymbol{c}$ are given by the usual relations

$$\tilde{c}_i = \sum_{j=1}^{i-1} \tilde{a}_{ij}, \quad c_i = \sum_{j=1}^{i} a_{ij}, \quad i = 1, \ldots, s.$$

To overcome the excessive numerical work for the solution of nonlinear systems, an essential gain is obtained by the approach proposed in [1]. We rewrite the semidiscrete formulation (3.5) in the form

$$\begin{aligned} \frac{\mathrm{d}}{\mathrm{d}t}\tilde{\boldsymbol{U}} &= \boldsymbol{\mathcal{K}}\big(\tilde{\boldsymbol{U}}, \boldsymbol{U}, t\big), \\ \frac{\mathrm{d}}{\mathrm{d}t}\boldsymbol{U} &= \boldsymbol{\mathcal{K}}\big(\tilde{\boldsymbol{U}}, \boldsymbol{U}, t\big), \end{aligned}$$

with initial condition $\tilde{\boldsymbol{w}}_j(0) = \boldsymbol{w}_j(0) = \boldsymbol{w}(x_j, 0)$, $j = 1, \ldots, M$, where we use the notation

$$\boldsymbol{\mathcal{K}}\big(\tilde{\boldsymbol{U}}, \boldsymbol{U}, t\big) := \boldsymbol{\mathcal{L}}\big(\tilde{\boldsymbol{U}}, t\big) + \frac{1}{\Delta z^2}\boldsymbol{\mathcal{B}}\big(\tilde{\boldsymbol{U}}\big)\boldsymbol{U},$$

with the aim of applying a partitioned Runge-Kutta scheme, consisting in the application of the explicit part to the first block of equations and the implicit part to the second block. If both Butcher arrays satisfy $\tilde{\boldsymbol{b}} = \boldsymbol{b}$, then the step from t^n to $t^{n+1} = t^n + \Delta t$ of the linearly implicit IMEX-RK scheme is given by the following algorithm.

Algorithm 3.1 (Linearly implicit IMEX-RK scheme)**.**

Input: approximate solution vector $\boldsymbol{U}^n$ *for* $t = t^n$

do $i = 1, \ldots, s$

compute the stage values:

$$\tilde{\boldsymbol{U}}^{(i)} \leftarrow \boldsymbol{U}^n + \Delta t \sum_{j=1}^{i-1} \tilde{a}_{ij}\boldsymbol{K}_j, \quad \hat{\boldsymbol{U}}^{(i)} \leftarrow \boldsymbol{U}^n + \Delta t \sum_{j=1}^{i-1} a_{ij}\boldsymbol{K}_j$$

solve for $\boldsymbol{K}_i$ *the linear equation*

$$\boldsymbol{K}_i = \boldsymbol{\mathcal{L}}\big(\tilde{\boldsymbol{U}}^{(i)}\big) + \frac{1}{\Delta z^2}\boldsymbol{\mathcal{B}}\big(\tilde{\boldsymbol{U}}^{(i)}\big)\big(\hat{\boldsymbol{U}}^{(i)} + \Delta t a_{ii}\boldsymbol{K}_i\big),$$

enddo

$$\boldsymbol{U}^{n+1} \leftarrow \boldsymbol{U}^n + \Delta t \sum_{j=1}^{s} b_j \boldsymbol{K}_j$$

Output: approximate solution vector $\boldsymbol{U}^{n+1}$ *for* $t = t^{n+1} = t^n + \Delta t$.

The linear equation for $\boldsymbol{K}_i$ is solved by using standard and efficient block tridiagonal solvers (see [10]).

In our experiments we use the classical second-order IMEX-RK scheme given by the following Butcher arrays:

$$\begin{array}{c|c} \tilde{\boldsymbol{c}} & \tilde{\boldsymbol{A}} \\ \hline & \tilde{\boldsymbol{b}}^{\mathrm{T}} \end{array} = \begin{array}{c|cc} 0 & 0 & 0 \\ 1 & 1 & 0 \\ \hline & 1/2 & 1/2 \end{array}, \qquad \begin{array}{c|c} \boldsymbol{c} & \boldsymbol{A} \\ \hline & \boldsymbol{b}^{\mathrm{T}} \end{array} = \begin{array}{c|cc} 0 & 0 & 0 \\ 1 & 1/2 & 1/2 \\ \hline & 1/2 & 1/2 \end{array},$$

denoted by H-CN(2,2,2) in [1], since it is a natural choice when dealing with convection-diffusion problems, since Heun's method is an SSP explicit RK one [11], and the Crank-Nicolson method is A-stable and widely used for diffusion problems.

4. Numerical experiments

4.1. Preliminaries

In this section we perform several numerical experiments to illustrate the behavior of the proposed IMEX-WENO scheme. Specifically, we consider the simulation of a three-component mixture proposed in [17].

Displacement chromatography (see, e.g., [19, 21]) relies on the idea that one component (the displacer) has a stronger affinity to the solid phase than any of the other components in the sample mixture, hence it has the capability to displace the other components of the mixture from the stationary phase. For a sufficiently long column and appropriate adsorption isotherms, the concentrations of the components form rectangular regions of high concentration of one component in the mixture. The series of such zones are the so-called isotachic train [5]. We consider the case of a mixture of two components and one displacer proposed in [17, Sect. 4.3]. The values of the parameters are: $\alpha_1 = 4, \alpha_2 = 5, \alpha_3 = 6, \beta_1 = 4, \beta_2 = 5, \beta_3 = 1$. In addition $\varepsilon = 0.5$ and $u = 0.2$.

For each iteration, Δt is determined by (3.6), (3.7) with the appropriate parameters $C_0 = C_1 = 1$. Moreover, we compute approximate L^1 errors at different times for each scheme as follows. We denote by $(c^M_{j,i}(t))_{j=1}^M$ and $(c^{\mathrm{ref}}_{l,i}(t))_{l=1}^{M_{\mathrm{ref}}}$ the numerical solution for the i-th component at time t calculated with M and $M_{\mathrm{ref}} = 12800$ cells, respectively. We compute $\tilde{c}^{\mathrm{ref}}_{j,i}(t)$ for $j = 1, \dots, M$ by

$$\tilde{c}^{\mathrm{ref}}_{j,i}(t) = \frac{1}{R}\sum_{k=1}^{R} c^{\mathrm{ref}}_{R(j-1)+k,i}(t), \quad R = M_{\mathrm{ref}}/M.$$

The total approximate L^1 error $(c^M_{j,i}(t))_{j=1}^M$ at time t is then given by

$$e^{\mathrm{tot}}_M(t) := \frac{1}{M}\sum_{i=1}^{N}\sum_{j=1}^{M}\left|\tilde{c}^{\mathrm{ref}}_{j,i}(t) - c^M_{j,i}(t)\right|.$$

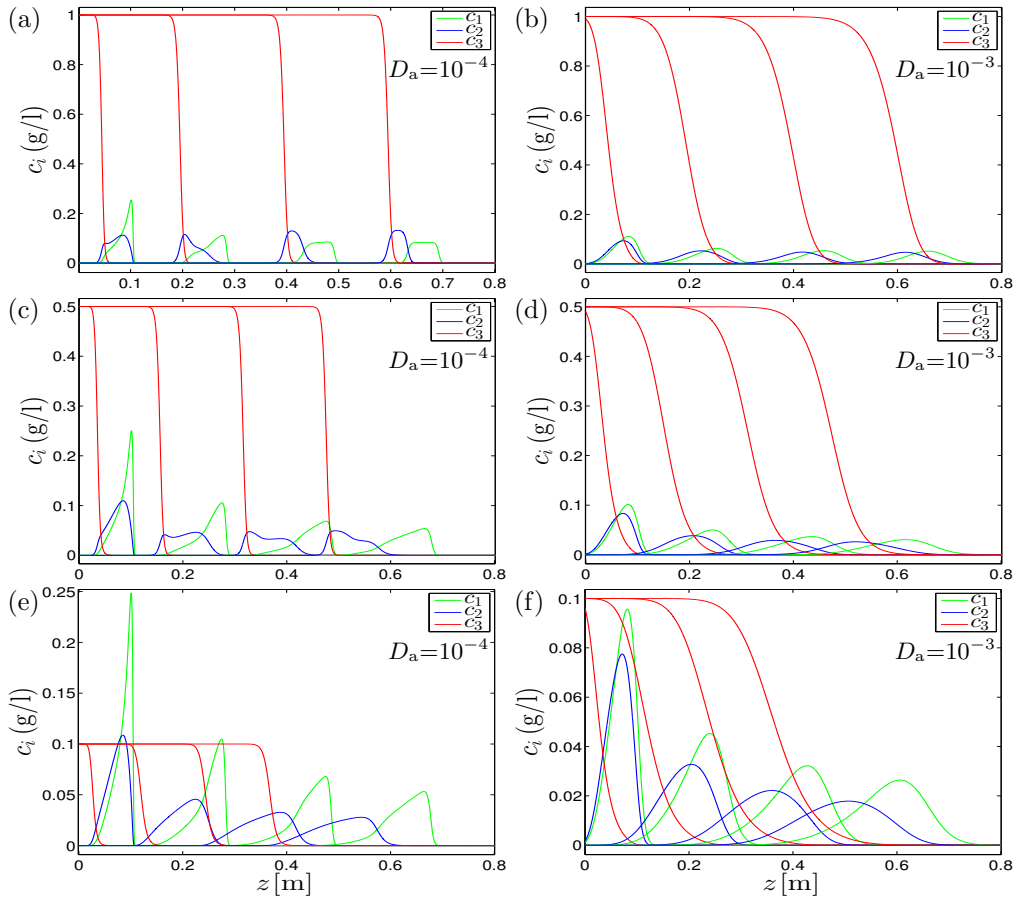

Figure 1: Reference numerical solution obtained by IMEX-RK2 at final times $T = 1, 4, 8, 12$ for (a, b) Experiment 1, (c, d) Experiment 2 and (e, f) Experiment 3.

Based on these approximate total errors, we may calculate a numerical order of convergence from pairs $e^{\text{tot}}_{M/2}(t)$ and $e^{\text{tot}}_{M}(t)$ by

$$\theta_M(t) := \log_2\big(e^{\text{tot}}_{M/2}(t)/e^{\text{tot}}_{M}(t)\big).$$

4.2. Three-component displacement tests

Experiment 1

We assume that components 1 and 2 are injected between $t = 0$ and $t = 0.1$ with $c_1 = c_2 = 1$ at $z = 0$. Component 3, the displacer, is injected

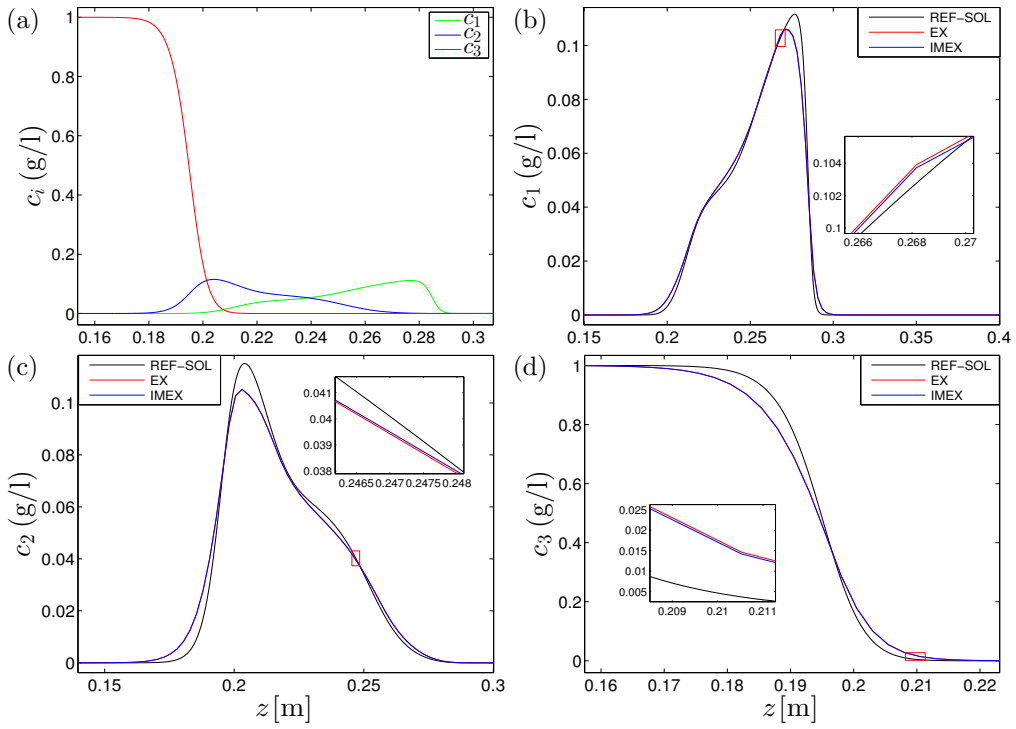

Figure 2: Experiment 1: numerical solutions obtained by IMEX-RK2 and explicit methods with $D_a = 10^{-4}$ at final time $T = 4$. Here and in Figures 3 to 7, the spatial resolution corresponds to $M = 400$, results are labeled by "IMEX" and "EX", and the reference solution ("REF-SOL") is defined by $M_{ref} = 12800$.

from $t = 0.1$ with $c_3 = 1$, that is,

$$\boldsymbol{c}_{inj}(t) = \begin{cases} (1,1,0)^T & \text{for } 0 \le t \le 0.1, \\ (0,0,1)^T & \text{for } t > 0.1. \end{cases}$$

Figures 1 (a) and (b) show the results for Experiment 1 for $D_a = 10^{-4}$ and $D_a = 10^{-3}$, respectively, obtained by the IMEX-RK scheme for the reference resolution $M = M_{ref} = 12800$. The formation of the displacement train can be clearly appreciated in both simulations. This fact (see [17]) prevents the formation of a rectangular pulse for component 1. This makes that only the second component can form a rectangular pulse. We see that the numerical solution behaves as expected.

Figures 2 and 3 display the numerical solution at times $T = 4$ and $T = 12$, respectively, obtained by both schemes (the explicit and the linearly implicit

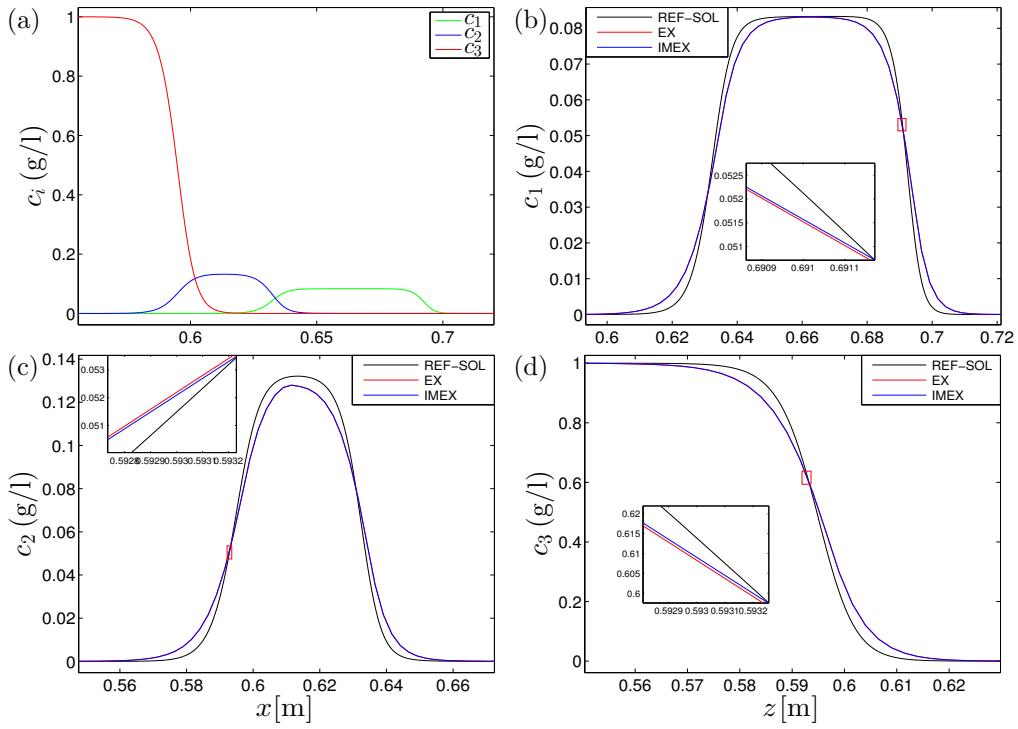

Figure 3: Experiment 1: numerical solutions for $D_{\mathrm{a}} = 10^{-4}$ and final time $T = 12$.

IMEX-RK scheme, denoted henceforth by "IMEX-RK2") at an intermediate spatial discretization $M = 400$ and with $D_{\mathrm{a}} = 10^{-4}$, while Table 1 shows the corresponding approximate errors and CPU times for both $D_{\mathrm{a}} = 10^{-4}$ and $D_{\mathrm{a}} = 10^{-3}$. Both figures, as well as Table 1, indicate that the explicit and IMEX-RK2 schemes produce numerical solutions of nearly the same quality; however, both numerical solutions are significantly more "smeared out" than the reference solution, which becomes especially appreciable near transitions between zones of slow variation and steep gradients.

Since $\boldsymbol{c}_{\mathrm{inj}}(t)$ is discontinuous at $t = 0.1$ here and in Experiments 2 and 3, we avoid a loss of order of accuracy in the time integration by ensuring that $t_n = 0.1$ for some intermediate n, by shortening Δt accordingly.

	Explicit			IMEX-RK2			Explicit			IMEX-RK2		
M	e_M^{tot}	θ_M	cpu	e_M^{tot}	θ_M	cpu	e_M^{tot}	θ_M	cpu	e_M^{tot}	θ_M	cpu
	Experiment 1, $D_{\mathrm{a}} = 10^{-4}$, $T = 4$						Experiment 1, $D_{\mathrm{a}} = 10^{-3}$, $T = 4$					
50	160.58	—	0.00	155.64	—	0.01	65.18	—	0.00	63.80	—	0.01
100	85.93	0.90	0.01	84.93	0.87	0.03	21.37	1.61	0.03	21.29	1.58	0.03
200	42.82	1.00	0.09	42.67	0.99	0.23	6.00	1.83	0.23	5.97	1.83	0.14
400	16.66	1.36	0.66	16.82	1.34	1.12	1.50	2.00	1.60	1.50	1.99	0.82
800	5.16	1.69	3.69	5.26	1.68	5.06	0.37	2.03	17.93	0.37	2.02	5.40
1600	1.34	1.94	22.77	1.41	1.90	22.28	0.09	2.04	119.73	0.09	2.01	18.62
	Experiment 1, $D_{\mathrm{a}} = 10^{-4}$, $T = 12$						Experiment 1, $D_{\mathrm{a}} = 10^{-3}$, $T = 12$					
50	207.58	—	0.01	207.96	—	0.03	71.15	—	0.02	71.00	—	0.03
100	115.32	0.85	0.05	115.90	0.84	0.11	21.96	1.70	0.09	22.00	1.69	0.10
200	52.88	1.12	0.29	53.194	1.12	0.50	5.80	1.92	0.73	5.82	1.92	0.43
400	19.81	1.42	1.52	19.98	1.41	2.45	1.45	2.00	4.43	1.45	2.00	2.36
800	6.02	1.72	9.82	6.09	1.71	13.67	0.36	2.01	51.05	0.36	2.02	11.72
1600	1.56	1.94	68.56	1.59	1.94	62.19	0.09	2.02	295.10	0.09	2.04	44.16

Table 1: Experiment 1: approximate L^1 errors (e_M^{tot}, figures to be multiplied by 10^{-3}), convergence rates (θ_M) and CPU times (cpu) in seconds.

Experiment 2

Next, we assume that the concentration injected for the displacer is further reduced, so that

$$\boldsymbol{c}_{\mathrm{inj}}(t) = \begin{cases} (1,1,0)^{\mathrm{T}} & \text{for } 0 \le t \le 0.1, \\ (0,0,0.5)^{\mathrm{T}} & \text{for } t > 0.1. \end{cases}$$

The values of the rest of the parameters are the same as in Experiment 1. In this case, none of the isotherms is intersected by the operating line and both components fail to form equilibrated rectangular pulses. The results of the reference solution are shown in Figures 1 (c) and (d), Figures 4 and 5 display numerical solutions for $M = 400$, and Table 2 provides the corresponding error and CPU time information.

Experiment 3

The concentration injected for the displacer is even further reduced, so that

$$\boldsymbol{c}_{\mathrm{inj}}(t) = \begin{cases} (1,1,0)^{\mathrm{T}} & \text{for } 0 \le t \le 0.1, \\ (0,0,0.1)^{\mathrm{T}} & \text{for } t > 0.1. \end{cases}$$

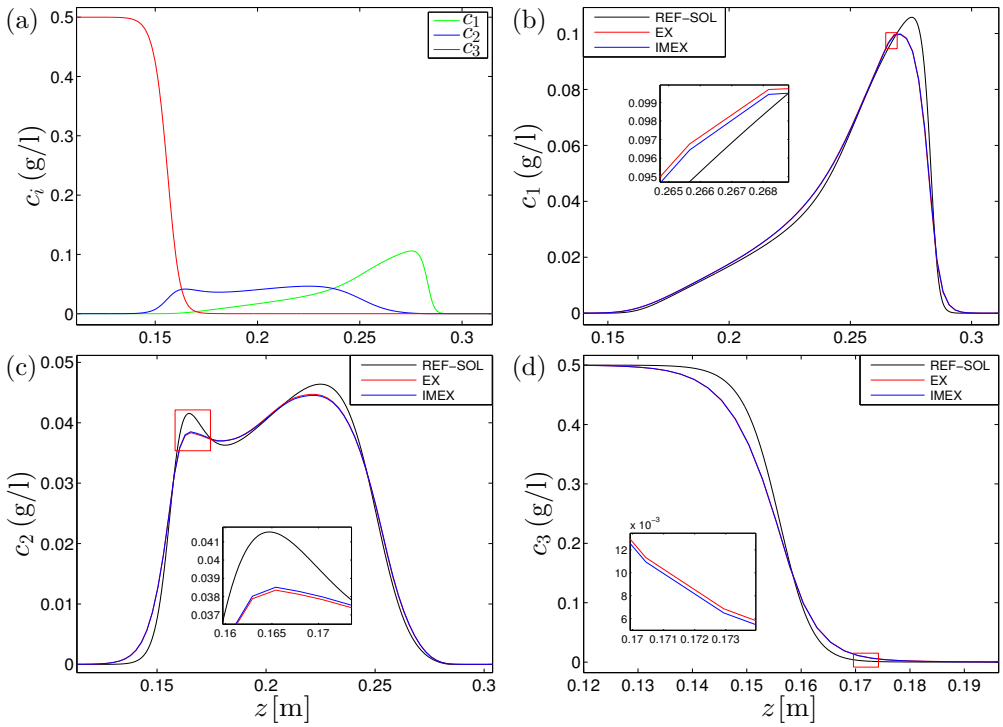

Figure 4: Experiment 2: numerical solutions for $D_{\mathrm{a}} = 10^{-4}$ and final time $T = 4$.

The values of the rest of the parameters are the same as in Experiments 1 and 2. In this case, none of the isotherms is intersected by the operating line. According to this, both components fail to form equilibrated rectangular pulses. The results of the reference solution are shown in Figure 1 (e) and (f), Figures 6 and 7 display numerical solutions for $M = 400$, and Table 3 provides the corresponding error and CPU time information.

4.3. Numerical error and efficiency

To assess the numerical error and efficiency of the linearly implicit IMEX-RK scheme we utilize the information of Tables 1, 2 and 3 for the final times $T = 4$ and $T = 12$ and the alternative diffusion coefficients $D_{\mathrm{a}} = 10^{-4}$ and $D_{\mathrm{a}} = 10^{-3}$. First of all, this information corroborates what can be inferred from Figures 2 to 7, namely that the explicit and IMEX-RK2 schemes produce almost the same errors, and moreover the observed rates of convergence θ_M are consistent with the fact that both schemes are formally second order in space and time (where we recall that the MUSCL extrapolation (3.3)

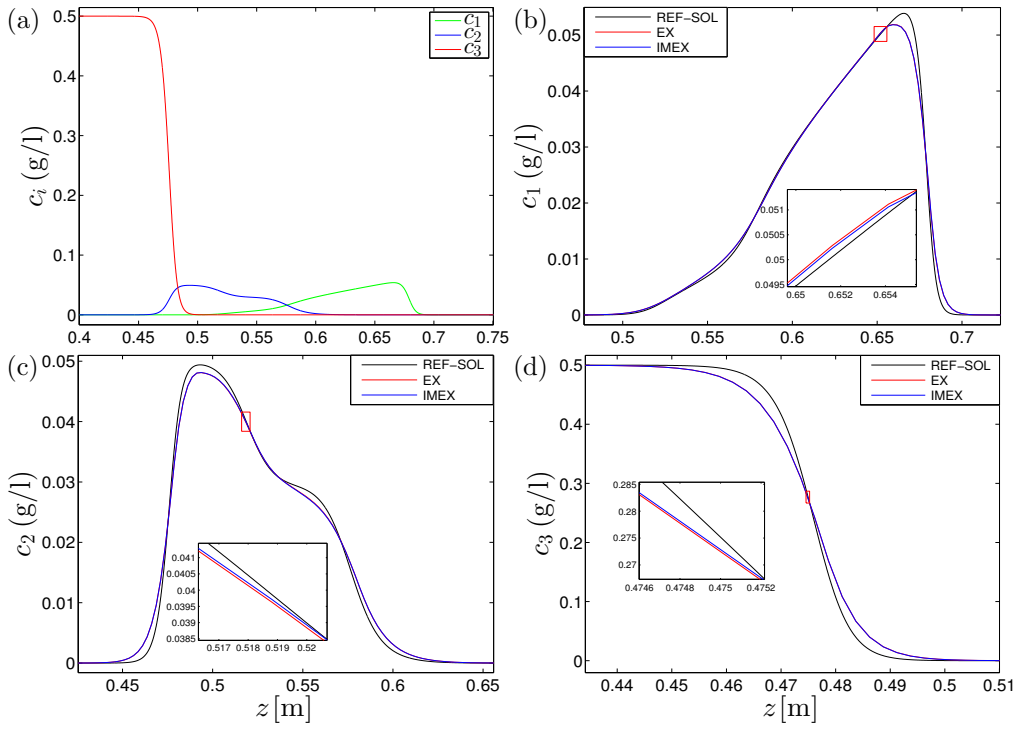

Figure 5: Experiment 2: numerical solutions for $D_a = 10^{-4}$ and final time $T = 12$.

is inactive near local extrema of the numerical solution, where the scheme locally degenerates to first-order accuracy). Furthermore, consistently with the respective CFL conditions (3.6) and (3.7) for the explicit and IMEX-RK2 schemes we observe that although each time step is computationally more involved for the IMEX-RK2 than for the explicit scheme, the IMEX-RK2 becomes faster than the explicit one for sufficiently fine discretizations. This gain is more significant, and becomes visible already for coarser discretizations, for the larger of the diffusion coefficients chosen for inspection.

The same observation can be deduced from Figures 8 and 9, where we present a number of efficiency plots, that is, of approximate L^1 error versus CPU time, deduced from the error and CPU time information of Tables 1 to 3. Here we understand by efficiency the amount of computational effort necessary to achieve a reduction of numerical error.

	Explicit			IMEX-RK2			Explicit			IMEX-RK2		
M	e_M^{tot}	θ_M	cpu	e_M^{tot}	θ_M	cpu	e_M^{tot}	θ_M	cpu	e_M^{tot}	θ_M	cpu
	Experiment 2, $D_{\text{a}} = 10^{-4}$, $T = 4$						Experiment 2, $D_{\text{a}} = 10^{-3}$, $T = 4$					
50	134.47	—	0.00	125.24	—	0.01	49.78	—	0.01	48.12	—	0.01
100	68.05	0.98	0.02	66.02	0.92	0.04	16.14	1.63	0.04	16.60	1.54	0.03
200	33.06	1.04	0.24	32.17	1.04	0.39	4.65	1.79	0.28	4.85	1.77	0.17
400	12.37	1.42	0.86	12.47	1.37	1.55	1.18	1.98	2.22	1.26	1.95	0.86
800	3.78	1.71	5.40	3.88	1.68	5.42	0.29	2.03	17.82	0.32	1.98	4.09
1600	0.99	1.93	23.11	1.04	1.90	17.06	0.07	2.04	123.10	0.09	1.88	16.77
	Experiment 2, $D_{\text{a}} = 10^{-4}$, $T = 12$						Experiment 2, $D_{\text{a}} = 10^{-3}$, $T = 12$					
50	144.53	—	0.02	142.59	—	0.04	49.94	—	0.03	49.25	—	0.04
100	66.31	1.12	0.09	66.39	1.10	0.13	15.33	1.70	0.13	15.39	1.68	0.13
200	30.63	1.11	0.43	30.62	1.12	0.71	4.08	1.91	0.89	4.09	1.91	0.49
400	11.16	1.46	1.89	11.24	1.45	3.17	1.02	2.00	5.60	1.02	2.00	2.28
800	3.29	1.76	12.63	3.40	1.72	3.67	0.25	2.02	48.94	0.25	2.02	10.24
1600	0.84	1.97	63.33	0.90	1.92	47.57	0.06	2.03	306.46	0.06	2.00	42.23

Table 2: Experiment 2: approximate L^1 errors (e_M^{tot}, figures to be multiplied by 10^{-3}), convergence rates (θ_M) and CPU times (cpu) in seconds.

5. Conclusions

Linearly implicit IMEX-RK methods were recently advanced as a tool for the efficient numerical solution of diffusively corrected multispecies kinematic flow models with applications to traffic flow and polydisperse sedimentation [1, 2, 4]. It has been demonstrated that these methods can also be applied to the ED model of chromatography, and they share the advantage of conservativity with the class of methods introduced in [7]. Moreover it turns out that they are competitive in accuracy with explicit methods of the same formal order of accuracy in space and time, and that they are more efficient than comparable explicit methods for relatively large diffusion coefficients and fine discretizations. Future work will explore the options of further increasing efficiency by alternative choices of underlying Runge-Kutta schemes, and by applying these methods to scenarios with degenerate or discontinuous diffusion coefficients, which were the prime motivation of our above-cited previous treatments.

Acknowledgements

RB is supported by Fondecyt project 1170473; CRHIAM, project Conicyt/FONDAP/15130015; and Fondef project ID15I10291. PM is supported

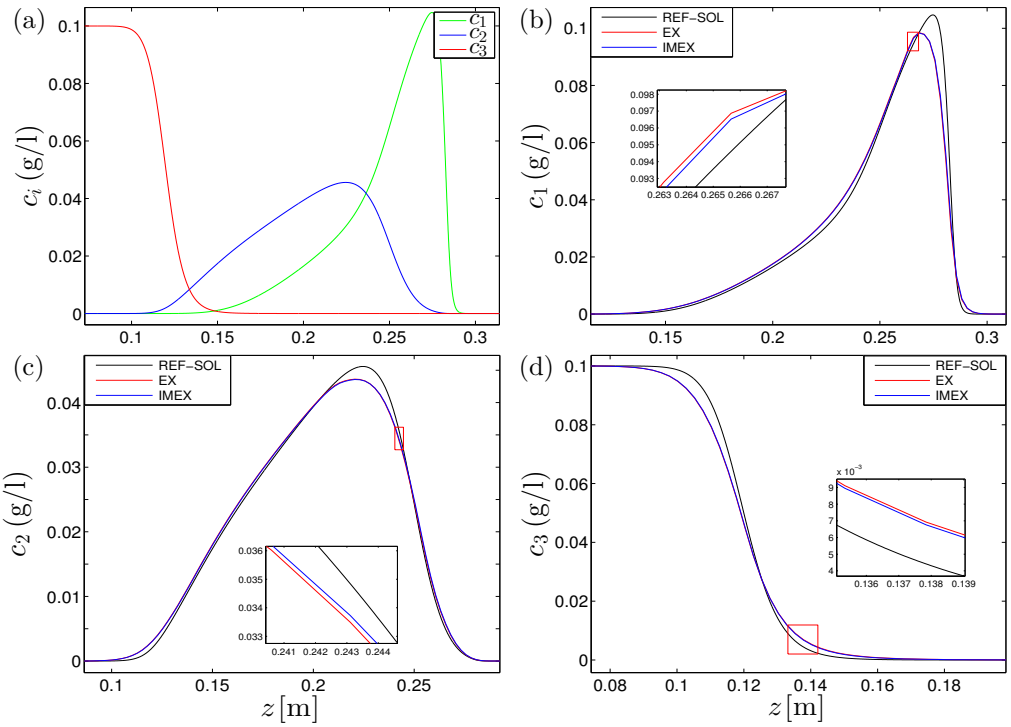

Figure 6: Experiment 3: numerical solutions for $D_{\mathrm{a}} = 10^{-4}$ and final time $T = 4$.

by Spanish MINECO projects MTM2014-54388-P and Conicyt (Chile), project PAI-MEC, folio 80150006. LR is supported by Conicyt scholarship. MS is supported by Fondecyt project 1140676. RB and MS also acknowledge support by BASAL project CMM, Universidad de Chile and Centro de Investigación en Ingeniería Matemática (CI^{2}MA), Universidad de Concepción, and by Conicyt project Anillo ACT1118 (ANANUM).

References

[1] S. Boscarino, R. Bürger, P. Mulet, G. Russo, L. M. Villada, Linearly implicit IMEX Runge-Kutta methods for a class of degenerate convection-diffusion problems, SIAM J. Sci. Comput. 37 (2015) B305–B331.

[2] S. Boscarino, R. Bürger, P. Mulet, G. Russo, L. M. Villada, On linearly implicit IMEX Runge-Kutta Methods for degenerate convection-diffusion problems modelling polydisperse sedimentation, Bull. Braz. Math. Soc. (N. S.) 47 (2016) 171–185.

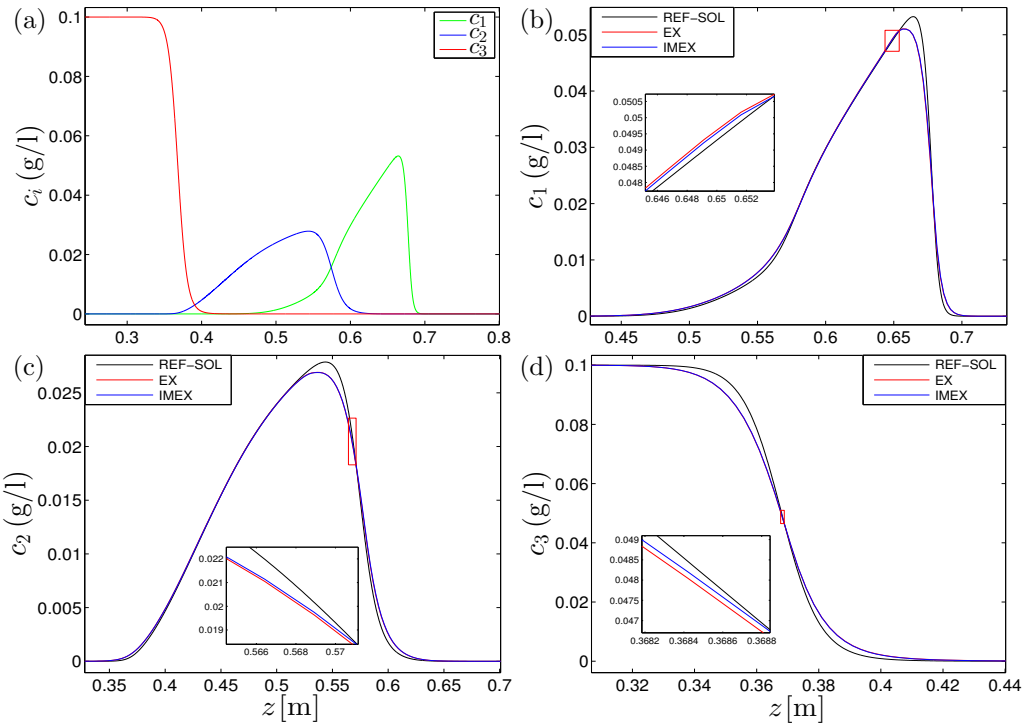

Figure 7: Experiment 3: numerical solutions for $D_{\mathrm{a}} = 10^{-4}$ and final time $T = 12$.

[3] C. Bourdarias, M. Gisclon, S. Junca, Existence of weak entropy solutions for gas chromatography system with one or two active species and non convex isotherms, Commun. Math. Sci. 5 (2007) 67–84.

[4] R. Bürger, P. Mulet, L. M. Villada, Regularized nonlinear solvers for IMEX methods applied to diffusively corrected multispecies kinematic flow models, SIAM J. Sci. Comput. 35 (2013) B751–B777.

[5] J. Cazes, Encyclopedia of Chromatography, Den New Dekker Encyclopedias. Taylor & Francis, 2001.

[6] R. Donat, F. Guerrero, P. Mulet, IMEX WENO schemes for two-phase flow vertical equilibrium processes in a homogeneous porous medium, Appl. Math. Inf. Sci. 7 (2013) 1865–1878.

[7] R. Donat, F. Guerrero, P. Mulet, Implicit-Explicit WENO scheme for

	Explicit			IMEX-RK2			Explicit			IMEX-RK2		
M	e_M^{tot}	θ_M	cpu	e_M^{tot}	θ_M	cpu	e_M^{tot}	θ_M	cpu	e_M^{tot}	θ_M	cpu
	Experiment 3, $D_{\text{a}} = 10^{-4}$, $T = 4$						Experiment 3, $D_{\text{a}} = 10^{-3}$, $T = 4$					
50	103.44	—	0.00	99.21	—	0.01	33.90	—	0.01	31.96	—	0.01
100	56.51	0.8	0.02	53.57	0.89	0.04	10.05	1.75	0.03	10.85	1.56	0.03
200	25.37	1.16	0.13	23.81	1.17	0.25	2.90	1.79	0.24	3.36	1.69	0.18
400	8.88	1.51	0.77	8.55	1.48	1.29	0.78	1.89	1.92	0.95	1.82	0.85
800	2.50	1.83	5.32	2.60	1.71	4.73	0.20	1.97	18.06	0.26	1.86	4.27
1600	0.61	2.03	19.74	0.68	1.93	16.92	0.05	2.01	120.61	0.08	1.70	17.13
	Experiment 3, $D_{\text{a}} = 10^{-4}$, $T = 12$						Experiment 3, $D_{\text{a}} = 10^{-3}$, $T = 12$					
50	107.30	—	0.02	105.66	—	0.03	28.63	—	0.03	28.16	—	0.03
100	51.06	1.07	0.06	49.20	1.10	0.12	8.42	1.77	0.11	8.79	1.68	0.11
200	20.08	1.35	0.34	19.32	1.35	0.55	2.27	1.89	0.73	2.44	1.85	0.54
400	6.97	1.53	1.91	6.84	1.50	2.75	0.58	1.96	5.17	0.65	1.92	2.21
800	1.93	1.85	14.60	2.04	1.75	12.36	0.15	2.00	46.85	0.17	1.93	10.40
1600	0.47	2.05	59.07	0.53	1.94	49.78	0.04	2.02	296.05	0.05	1.77	42.45

Table 3: Experiment 3: approximate L^1 errors (e_M^{tot}, figures to be multiplied by 10^{-3}), convergence rates (θ_M) and CPU times (cpu) in seconds.

the equilibrium dispersive model of chromatography. Preprint, 2017, available from `arXiv.org`.

[8] R. Donat, P. Mulet, A secular equation for the Jacobian matrix of certain multispecies kinematic flow models, Numer. Methods Partial Differential Equations 26 (2010) 159–175.

[9] S. D. Eidelman, N. V. Zhitarashu. Parabolic Boundary Value Problems, Birkhäuser Verlag, Basel, 1998.

[10] G.H. Golub, C.F. van Loan, Matrix Computations, The Johns Hopkins University Press, 1996.

[11] S. Gottlieb, C.-W. Shu, E. Tadmor, Strong stability-preserving high-order time discretization methods, SIAM Rev. 43 (2001) 89–112.

[12] G. Guiochon, G. Shirazi, M. Katti, Fundamentals of Preparative and Nonlinear Chromatography, Second Ed., Elsevier, 2006.

[13] F. James, Convergence results for some conservation laws with a reflux boundary condition and a relaxation term arising in chemical engineering, SIAM J. Math. Anal. 29 (1998) 1200–1223.

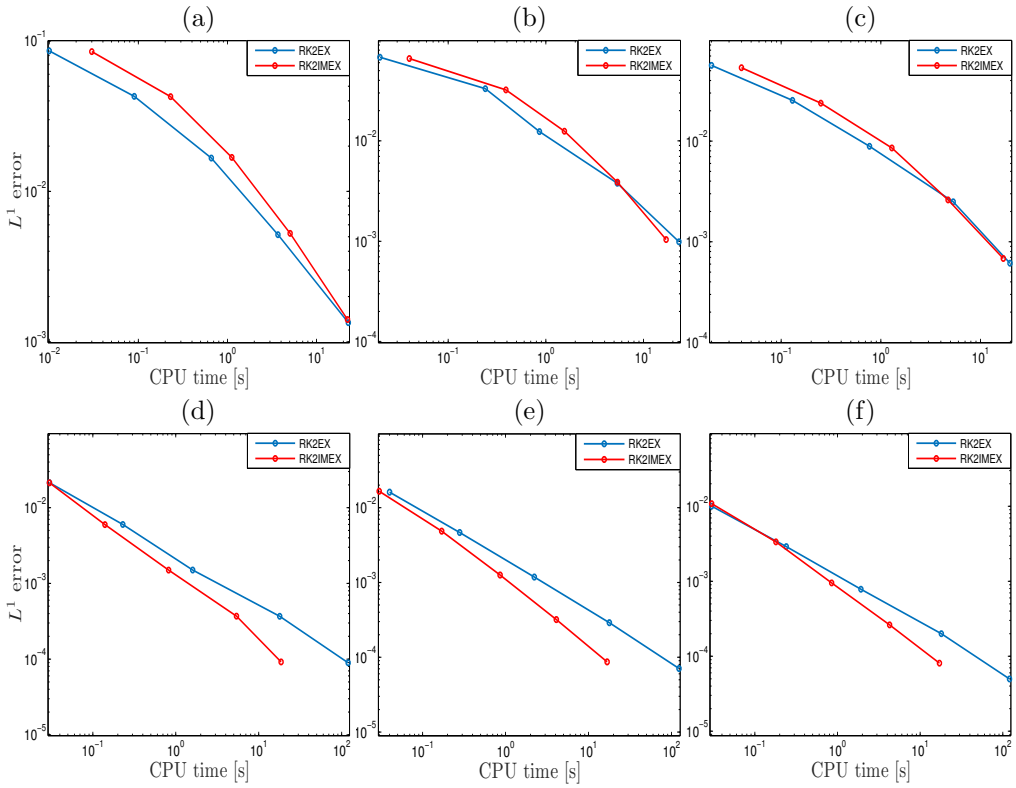

Figure 8: Efficiency plots for (a, d) Experiment 1, (b, e) Experiment 2 and (c, f) Experiment 3 with (a, b, c) $D_{\mathrm{a}} = 10^{-4}$, (d, e, f) $D_{\mathrm{a}} = 10^{-3}$ and final time $T = 4$.

[14] F. James, M. Postel, M. Sepúlveda, Numerical comparison between relaxation and nonlinear equilibrium models. Application to chemical engineering, Physica D: Nonlin. Phen. 138 (2000) 316–333.

[15] F. James, M. Sepúlveda, P. Valentin, Statistical thermodynamics models for multicomponent isothermal diphasic equilibria, Math. Models Methods Appl. Sci. 7 (1997) 1–29.

[16] F. James, M. Sepúlveda, F. Charton, I. Quiñones, G. Guiochon. Determination of binary competitive equilibrium isotherms from the individual chromatographic band profiles, Chem. Eng. Sci. 54 (1999) 1677–1696.

[17] S. Javeed, A. Qamar, A. Seidel-Morgenstern, G. Warnecke, Efficient and

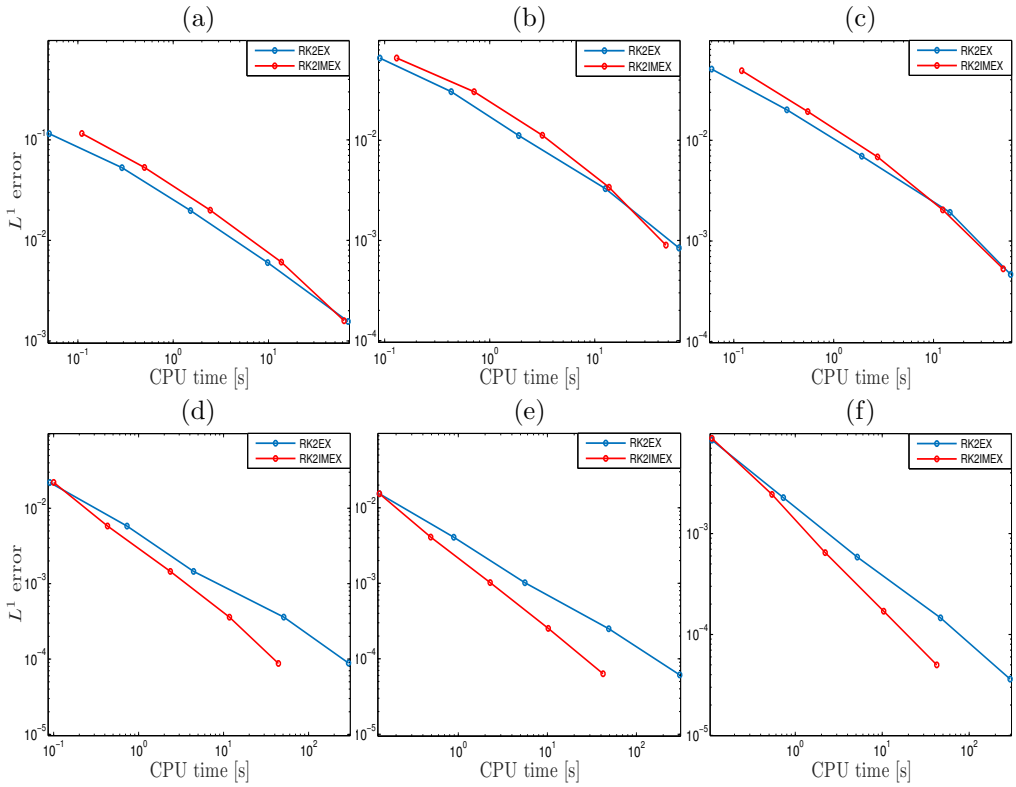

Figure 9: Efficiency plots for (a, d) Experiment 1, (b, e) Experiment 2 and (c, f) Experiment 3 with (a, b, c) $D_{\mathrm{a}} = 10^{-4}$, (d, e, f) $D_{\mathrm{a}} = 10^{-3}$ and final time $T = 12$.

accurate numerical simulation of nonlinear chromatographic processes, Comput. Chem. Eng. 35 (2011) 2294–2305.

[18] I. Langmuir, The adsorption of gases on plane surfaces of glass, mica and platinum, J. Amer. Chem. Soc. 40 (1918) 1361–1403.

[19] M.D. Le Van, G. Carta, C.M. Yan, Adsorption and Ion Exchange, Chapter 16 in R.H. Perry, D.W. Green and J.O. Maloney (Eds.), Perry's Chemical Engineer's Handbook, Seventh Edition, McGraw Hill, New York 1998, 16-1–16-66.

[20] M. Mazzotti, A. Rajendran, Equilibrium theory-based analysis of nonlinear waves in separation processes, Annu. Rev. Chem. Biomol. Eng. 4 (2013) 119–141.

[21] H.K. Rhee, R. Aris, N.R. Admundson, On the theory of multicomponent chromatography, Philos. Trans. Roy. Soc. London A267 (1970) 419–455.

[22] P. Rouchon, M. Schonauer, P. Valentin, G. Guiochon, Numerical simulation of band propagation in nonlinear chromatography, Separ. Sci. Technol. 22 (1987) 1793–1833.

[23] D.U. Staerk, A. Shitangkoon, E. Winchester, G. Vigh, A. Felinger, G. Guiochon, Use of the equilibrium-dispersive model of nonlinear gas chromatography for the modelling of the elution band profiles in the preparative-scale gas chromatographic separation of enantiomers, J. Chromatography A 734 (1996) 289–296.

[24] B. van Leer, Towards the ultimate conservative finite difference scheme, V. A second order sequel to Godunov's method, J. Comput. Phys. 32 (1979) 101–136.

Centro de Investigación en Ingeniería Matemática (CI^{2}MA)

PRE-PUBLICACIONES 2016 - 2017

2016-42 Jessika Camaño, Christopher Lackner, Peter Monk: *Electromagnetic Stekloff eigenvalues in inverse scattering*

2017-01 Raimund Bürger, Sudarshan K. Kenettinkara, David Zorío: *Approximate Lax-Wendroff discontinuous Galerkin methods for hyperbolic conservation laws*

2017-02 David Mora, Gonzalo Rivera, Iván Velásquez: *A virtual element method for the vibration problem of Kirchhoff plates*

2017-03 Carlos Garcia, Gabriel N. Gatica, Antonio Marquez, Salim Meddahi: *A fully discrete scheme for the pressure-stress formulation of the time-domain fluid-structure interaction problem*

2017-04 Luis F. Gatica, Filander A. Sequeira: *A priori and a posteriori error analyses of an HDG method for the Brinkman problem*

2017-05 Ernesto Cáceres, Gabriel N. Gatica, Filander A. Sequeira: *A mixed virtual element method for quasi-Newtonian Stokes flows*

2017-06 Celso R. B. Cabral, Luis M. Castro, Christian E. Galarza, Víctor H. Lachos: *Robust quantile regression using a generalized class of skewed distributions*

2017-07 Raimund Bürger, Julio Careaga, Stefan Diehl: *A simulation model for settling tanks with varying cross-sectional area*

2017-08 Raimund Bürger, Sudarshan K. Kenettinkara, Ricardo Ruiz-Baier, Hector Torres: *Non-conforming/DG coupled schemes for multicomponent viscous flow in porous media with adsorption*

2017-09 Thomas Führer, Norbert Heuer, Michael Karkulik, Rodolfo Rodríguez: *Combining the DPG method with finite elements*

2017-10 Cinthya Rivas, Rodolfo Rodríguez, Manuel Solano: *A perfectly matched layer for finite-element calculations of diffraction by metallic surface-relief gratings*

2017-11 Raimund Bürger, Pep Mulet, Lihki Rubio, Mauricio Sepúlveda: *Linearly implicit IMEX schemes for the equilibrium dispersive model of chromatography*

Para obtener copias de las Pre-Publicaciones, escribir o llamar a: Director, Centro de Investigación en Ingeniería Matemática, Universidad de Concepción, Casilla 160-C, Concepción, Chile, Tel.: 41-2661324, o bien, visitar la página web del centro: `http://www.ci2ma.udec.cl`







Centro de Investigación en
Ingeniería Matemática (CI²MA)
Universidad de Concepción

Casilla 160-C, Concepción, Chile
Tel.: 56-41-2661324/2661554/2661316
http://www.ci2ma.udec.cl